Experimental and Modeling Studies of B Atom Number Density Distributions in Hot Filament Activated B_2H_6/H_2 and $B_2H_6/CH_4/H_2$ Gas Mixtures†

Dane W. Comerford,‡ Andrew Cheesman,‡ Thomas P. F. Carpenter,‡ David M. E. Davies,‡ Neil A. Fox,‡ Rebecca S. Sage,‡ James A. Smith,‡ Michael N. R. Ashfold,*,‡ and Yuri A. Mankelevich§

School of Chemistry, University of Bristol, Bristol, U.K., BS8 1TS, and Nuclear Physics Institute, Moscow State University, 119992 Moscow, Russia

Received: June 25, 2005; In Final Form: August 26, 2005

Experimental and modeling studies of the gas-phase chemistry occurring in dilute, hot filament (HF) activated B_2H_6/H_2 and $B_2H_6/CH_4/H_2$ gas mixtures are reported. Spatially resolved relative number densities of B (and H) atoms have been measured by resonance enhanced multiphoton ionization methods, as a function of process conditions (e.g. the HF material and its temperature, the B_2H_6/H_2 mixing ratio, and the presence (or not) of added CH_4). Three-dimensional modeling of the H/B chemistry prevailing in such HF activated gas mixtures using a simplified representation of the gas phase chemistry succeeds in reproducing all of the experimentally observed trends, and in illustrating the key role of the "H-shifting" reactions $BH_x + H \rightleftharpoons BH_{x-1} + H_2$ ($x = 1-3$) in enabling rapid interconversion between the various BH_x ($x = 0-3$) species. CH_4 addition, at partial pressures appropriate for growth of boron-doped diamond by chemical vapor deposition methods, leads to ~30% reduction in the measured B atom signal near the HF. The modeling suggests that this is mainly due to concomitant H atom depletion near the HF, but it also allows us a first assessment of the possible contributions from B/C coupling reactions upon CH_4 addition to HF activated B_2H_6/H_2 gas mixtures.

Introduction

Addition of trace amounts of a boron containing precursor during chemical vapor deposition (CVD) of diamond thin films is of considerable interest, as incorporated B atoms act as acceptors ($E_a \sim 0.37$ eV) and impart p-type semiconductivity to the as-grown B-doped diamond.[1] B-doped CVD diamond finds use in intrinsic devices[2] and electrochemical sensors[3] and, when combined with P-doped diamond (an n-type semiconductor), as a UV light source.[4] Reports of n-type electrical conductivity from deuterated (100) B-doped diamond layers[5] have served to stimulate additional interest, though theory[6] has thus far failed to validate initial suggestions that such conductivity might be associated with boron−deuterium complex defects within the diamond lattice. Post-growth film characterization has revealed a marked preference for B incorporation in {111} rather than {100} growth sectors,[7,8] but the details of the underpinning gas-phase and gas−surface chemistry involved in the growth of B-doped CVD diamond are poorly understood.

We have embarked on a two pronged strategy aimed at rectifying some of these deficiencies. Aspects of the gas−surface chemistry are being explored via density functional theory (DFT) based electronic structure calculations. Thus far, our work in this area has focused on the addition of BH_x ($x = 1-3$) species to a small carbon cluster that traditionally has been used to mimic a small portion of the H-terminated 2×1 reconstructed diamond (100) surface.[9] This study is now being extended using a larger model of the diamond surface and a hybrid DFT/molecular mechanics scheme in which crucial atoms involved in the reaction site are treated quantum mechanically, but the scaffold of neighboring C atoms that makes up the larger diamond lattice is treated using classical force fields.

B_2H_6 is one of the more commonly used boron containing precursors in diamond CVD. Here we report combined experimental and modeling studies of the gas-phase chemistry occurring in dilute, hot filament (HF) activated, B_2H_6/H_2 gas mixtures, along with preliminary investigations of HF activated $B_2H_6/CH_4/H_2$ gas mixtures, as a precursor to future analyses of the full B/C/H gas-phase chemistry. The experimental part of this project has involved use of resonance enhanced multiphoton ionization (REMPI) techniques to measure spatially resolved relative number densities of B (and H) atoms, as a function of process conditions (e.g. the HF material, and its temperature, T_{fil}, the B_2H_6/H_2 mixing ratio, and the presence (or not) of added CH_4). It has also served to reveal unintended complications arising from the reactivity of B containing species with the hot metal filament. The complementary modeling builds on previous analyses of CH_4/H_2[10−13] and $CH_4/NH_3/H_2$[14] gas-phase chemistry in the Bristol HF reactors. The model comprises three blocks, which describe (i) activation of the reactive mixture (e.g. gas heating, catalytic H atom production and, in the present case, allows for loss of gas-phase boron by incorporation at the filament surface), (ii) gas-phase processes (heat and mass transfer, and chemical kinetics), and (iii) gas−surface processes at the substrate. The third block was not required here, as no substrate was present in any of the current experiments. Wherever possible, the necessary gas phase thermochemical and kinetic input has been taken from the literature.[15−17] As previously, [10,12,14] the conservation equations for mass, momentum, energy, and species concentrations, together with

† Part of the special issue "Jürgen Troe Festschrift".

* Author for correspondence. Telephone: (117)-9288312. Fax: (117)-9250612. E-mail: mike.ashfold@bris.ac.uk.

‡ University of Bristol.

§ Moscow State University.

10.1021/jp053455p CCC: $33.50
Published on Web 10/01/2005

appropriate initial and boundary conditions, thermal and caloric equations of state, are each integrated numerically until steady-state conditions are attained, thereby yielding spatial distributions of the gas temperature, T_{gas}, the flow field, and the H atom, BH_x species, and B_2H_6 number densities and mole fractions. The modeling, which succeeds in reproducing all of the trends observed experimentally, reveals rapid interconversion between the various BH_x ($x = 0-3$) species via successive H-shifting reactions and suggests concomitant H atom loss (rather than B/C coupling reactions) as the main cause of the observed reduction in the B atom density upon CH_4 addition to HF activated dilute B_2H_6/H_2 gas mixtures.

Experimental Section

The experimental apparatus and procedures have been described previously,[11,18] and so only key or new features are described here. The CVD chamber consists of a six-way cross, which is evacuable to a base pressure of $\sim 10^{-2}$ Torr using a two stage rotary pump connected to the lower arm. Three of the sidearms in the horizontal plane are fitted with quartz windows—two to allow exit and entrance of the REMPI laser radiation, while the third is an observation window that allows determination of T_{fil} using a two-color pyrometer (Land Infrared FRP12). The HF was made of Ta (or Re) wire (250 μm diameter, 7 turns with coil diameter $\sim$3 mm) and mounted so that its long axis was parallel to the laser propagation axis. Typically, a borodized Ta filament drawing 6.5 A at $\sim$12.5 V exhibited a color temperature of $\sim$2100 °C. Vertical translation (by $\leq$25 mm) relative to the fixed laser focus and ion probe was achieved by attaching the HF to the top flange via a linear transfer mechanism. H_2 (100 sccm), CH_4 (0−5 sccm), and B_2H_6 (0−1 sccm of a 4.75% B_2H_6 in H_2 mixture) were metered using separate mass flow controllers (MFCs, Tylan), and premixed in a manifold before introduction into the upper arm of the chamber, the total pressure in which was regulated at $p = 20$ Torr.

B atoms were detected by 2 + 1 REMPI on the $2s^24p^1;^2P^\circ \leftarrow 2s^22p^1;^2P^\circ$ transition at wavelengths $\sim$346.1 nm.[19,20] As illustrated in the following section, both states are affected by spin−orbit splitting, with the result that this transition appears as a pair of partially resolved doublets. The requisite probe wavelengths were generated using a Nd:YAG (Continuum Surelite II-10) laser operating at 10 Hz to pump a dye laser (Spectra-Physics PDL3) operating with a mixture of LDS 698 and DCM dyes, and subsequent frequency doubling using a KD*P crystal mounted in a home-built "auto-tracker". The frequency doubled UV light ($\sim$0.5 mJ pulse^{-1}, bandwidth $\sim$0.15 cm^{-1} (fwhm)) was separated from the fundamental radiation using a Pellin Broca prism, and then steered via a 90° prism and focused (25 cm focal length lens) to a spot close below the coiled HF and $\sim$1 mm from a biased probe wire (Pt, 0.5 mm diameter, −50 V) in the center of the chamber. Transient ion currents sampled by the probe wire were recorded with an oscilloscope (LeCroy 9450) and passed to a PC via a GPIB interface for collection and subsequent analysis using the in-house data collection program DRIVE.[21] Shot to shot (and longer term) variations in the intensity of the incident UV radiation were monitored by directing the UV beam exiting the chamber into a cuvette containing dilute rhodamine 6G solution; the resulting fluorescence was monitored by a photodiode and passed to another input channel of the oscilloscope to allow subsequent power normalization of the measured ion currents. Portions of the fundamental dye laser radiation initially separated by the Pellin Broca prism were separated further using beam splitters and sampled using a wavemeter (Coherent WaveMaster) and an etalon/photodiode combination to ensure accurate frequency calibration. H atoms were detected by REMPI also, by 2 + 1 REMPI on the $2s^1 \leftarrow 1s^1$ transition at $\sim$243 nm, as in the earlier work of Redman et al.[18]

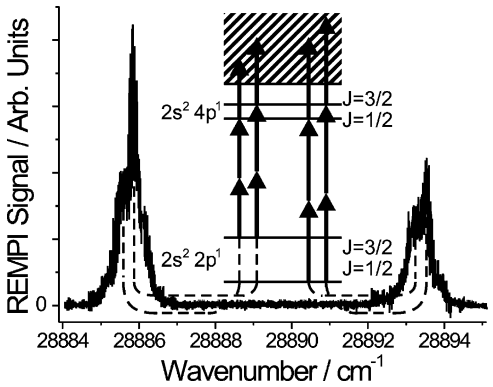

Figure 1. 2 + 1 REMPI spectrum of B atoms in a 0.0475% B_2H_6 in H_2 gas mixture activated with a borodized Ta HF; $p = 20$ Torr, $T_{fil} =$ 2100 °C, $d = 3$ mm. Details of the probe transitions are provided in the partial Grotrian diagram shown (not to scale) in the inset.

HFs were analyzed, after use, by scanning electron microscopy (SEM, using a JEOL JSM 5600LV instrument) and secondary ion mass spectroscopy (SIMS, using a substantially modified VG 7035 double focusing magnetic sector GCMS equipped with a FEI electronically variable aperture focused gallium ion gun operated within the Interface Analysis Centre at the University of Bristol).

B_2H_6/H_2: Experimental Measurements. The 2 + 1 REMPI spectra of atomic B have been reported previously, in the excitation wavelength range $350 < \lambda < 304$ nm, but only at comparatively low resolution.[20] Two possible REMPI detection schemes were investigated in the present work. The first involved 1 + 1 REMPI via the $2s^23s^1;^2S$ state at $\lambda \sim 249.7$ nm. One photon absorption on the $2s^23s^1;^2S \leftarrow 2s^22p^1;^2P^\circ$ transition has been used previously to monitor B atoms in dilute low-pressure $B_2H_6/H_2/Ar$ plasmas.[22] Detecting REMPI signals at this wavelength attributable to B atoms in dilute HF activated B_2H_6/H_2 gas mixtures was straightforward, but the measured line shapes were much broader than would be expected on the basis of the known laser bandwidth, Doppler broadening effects, etc. This we attribute to partial saturation of the initial one photon absorption, the cross-section for which we presume to be very much greater than that of the subsequent ionization step. Figure 1 shows the spectrum obtained following excitation at $\lambda \sim 346.1$ nm, with the probe laser focus at a distance $d = 3$ mm below the bottom of the HF. Ionization of B atoms at this wavelength is resonance enhanced by the $2s^24p^1;^2P^\circ$ state at the two photon energy. The relevant part of the Grotrian diagram, also shown in Figure 1, highlights the spin−orbit splitting present in both the ground and excited $^2P^\circ$ states. The spectrum takes the form of two partially resolved doublets. The large separation is due to the ground-state splitting (15.254 cm^{-1}), while the incompletely resolved doubling within each peak is due to spin−orbit splitting in the excited state (0.638 cm^{-1}).[19] The relative peak intensities reflect the differing transition strengths $\Gamma_{J'J''}$ which, in the case of multiplet transitions in a light atom (i.e., transitions that are well described using the Russell−Saunders coupling scheme), are given by

$$\Gamma_{J'J''} = (2J''+1)(2J'+1)\left|\begin{Bmatrix} L'' & J'' & S'' \\ J' & L' & k \end{Bmatrix}\right|^2, \qquad (1)$$

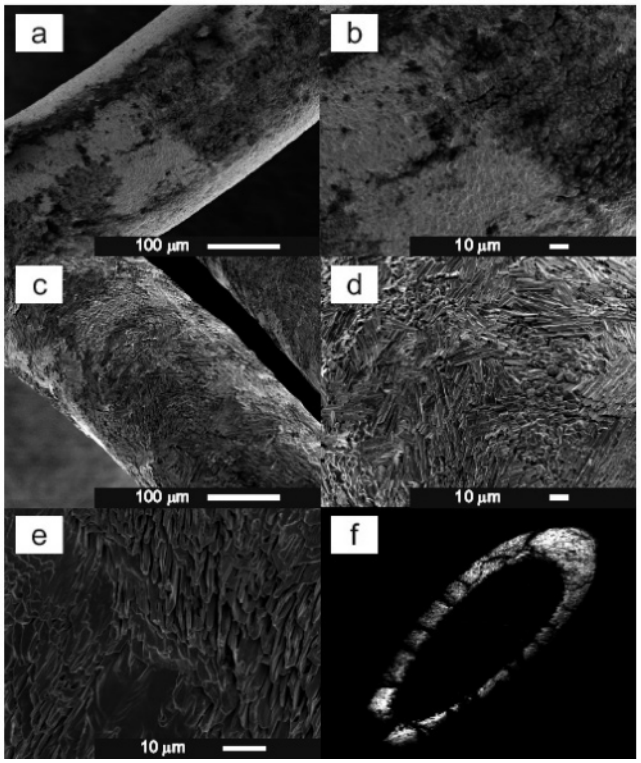

Figure 2. (a) Overview and (b) higher magnification SEM images of a Ta HF maintained at 1700 °C in a 0.0475% B_2H_6 in H_2 gas mixture for 4 h. (c and d) Analogous micrographs of a Ta HF run in the same gas mixture, for the same duration, but at 2100 °C. (e) Higher magnification image of a Ta HF held in a 0.0475% B_2H_6 in H_2 gas mixture at 2100 °C for 24 h. Evidence of surface melting and recrystallization is apparent in each of images c−e. (f) Cross-sectional view of a Ta HF maintained at 1700 °C in a 0.0475% B_2H_6 in H_2 gas mixture for 4 h, obtained by SIMS and monitoring just the B (*m*/*z* 10 and 11) signal. To record this image, the HF was potted in Struers' Polyfast resin, and polished using Kemet 6 and 1 μm pastes, resulting in the elliptical section shown.

where the *J*, *L*, and *S* atomic quantum numbers have their usual meanings, the term in curly brackets is a 6 − *j* symbol, and *k* is the rank of the transition tensor. $\Delta J \neq 0$ transitions are carried exclusively by rank $k = 2$ components. Only the $k = 0$ scalar term can contribute to the $J' = {}^1/_2 \leftarrow J'' = {}^1/_2$ transition, whereas components of both ranks can contribute to the $J' = {}^3/_2 \leftarrow J'' = {}^3/_2$ transition. Evaluation of eq 1 for the four possible transitions, and comparison with Figure 1, indicates that the $k = 0$ and $k = 2$ components make comparable contributions to the measured spectrum. The $(2J'' + 1)$ degeneracy term ensures that the lower wavenumber peak, associated with excitation of atoms in the higher energy ($^2P^\circ_{3/2}$) spin−orbit component of the ground state, is the more intense; at all gas temperatures relevant to the present work the degeneracy term far outweighs any small difference in population due to the Boltzmann factor. This peak was therefore used for all subsequent relative number density measurements.

The measured B atom signals can be sensitively dependent upon the choice of HF material, and any preconditioning strategy employed. Experiments with dilute B_2H_6/H_2 gas mixtures and a virgin Ta HF initially yielded no B atom signal. The required signal was found to develop with time, however, suggesting that the bare Ta HF reacts with, and acts as a local sink for, gas-phase B containing species. As Figure 2 shows, scanning electron microscopy (SEM), and secondary ion mass spectroscopy (SIMS) analysis confirm the progressive development of a boron containing surface layer on the Ta HF as time increases. The rate of loss of B diminishes with time but, as shown below, never decays to zero during the working lifetime of a Ta HF. Our standard operating procedure thus involved initial borodization by running the Ta HF in a 0.0475% B_2H_6 in H_2 gas mixture at the chosen T_{fil} for 6 h prior to making any measurements. The resulting embrittlement ensured that it was rarely possible to use such a borodized HF for more than 1 day. Prior carburization of a Ta HF (by operating the filament at elevated T_{fil} in a 1% CH_4/H_2 gas mixture for several hours prior to exposure to any B_2H_6) reduced the efficiency of the filament surface as a sink for boron. Rhenium was also investigated as a HF material. Re is significantly more expensive than Ta, but turns out to be a much less effective sink for boron and thus a more suitable HF material for activating B_2H_6/H_2 gas mixtures: B atom signals were immediately detectable in a Re HF activated 0.0475% B_2H_6 in H_2 gas mixture.

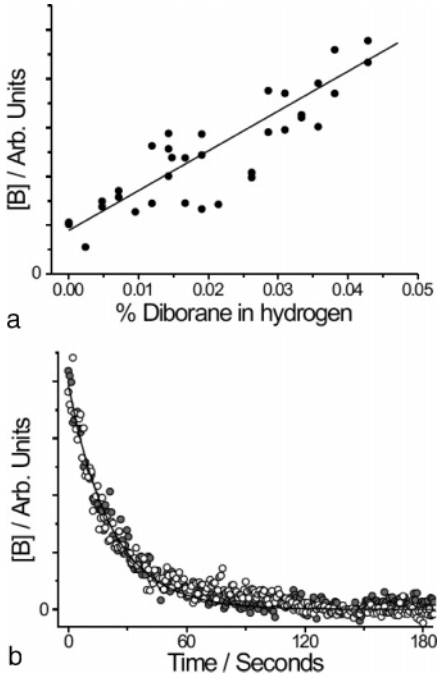

Figure 3. (a) Measured B atom signal (obtained as the area under the 2 + 1 REMPI line profile) plotted as a function of B_2H_6 fraction in a B_2H_6/H_2 gas mixture activated with a borodized Ta HF. (b) Plot of B atom signal (measured at the peak of the 28886 cm^{-1} feature) as a function of time after switching off the 1 sccm of 4.75% B_2H_6 in H_2 component to the total gas flow. The filled and opened circles represent data from two separate measurements. $p = 20$ Torr, $T_{fil} = 2100$ °C, H_2 flow rate = 100 sccm, and $d = 3$ mm in both cases.

Given the evident reactivity of boron with the Ta HF it was deemed prudent to test that the measured B atoms arise as a result of the intended gas-phase chemistry rather than, for example, thermal desorption from the borodized HF itself. Two data sets pertinent to this issue are shown in Figure 3. Figure 3a shows a plot of measured B atom signal as a function of B_2H_6 fraction in a B_2H_6/H_2 gas mixture, flowing at 100 sccm and at $p = 20$ Torr, activated with a borodized Ta HF ($T_{fil} =$ 2100 °C), probed at $d = 3$ mm. These should be taken as the standard operating conditions for all subsequent data sets, except where specified otherwise. Each point in this plot was obtained as follows: Having selected a B_2H_6 flow rate, the local gas composition was allowed to stabilize for ∼5 min, after which time the probe laser wavelength was scanned across the 28886 cm^{-1} feature. Each point within the measured spectrum was then normalized with respect to the instantaneous UV pulse

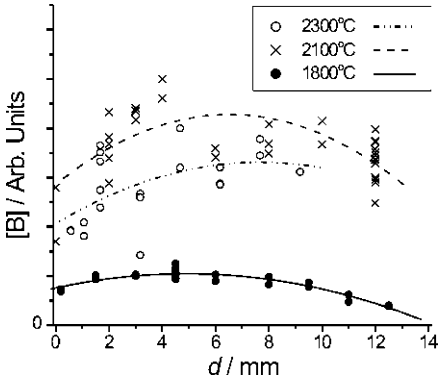

Figure 4. Plots of [B] vs d using borodized Ta HF, measured at the specified T_{fil} values. The superposed lines through the data are intended merely to guide the eye.

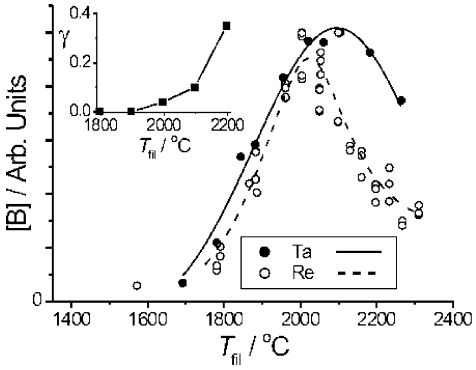

Figure 5. Plots of [B] vs T_{fil} using a borodized Ta HF (●) and a Re HF (○), measured at $d = 3$ mm. Lines through the data points are merely intended to guide the eye. The inset shows the T_{fil} dependence of the boron accommodation coefficient, γ, required by the modeling in order to reproduce these experimental trends.

energy, and the area under the resulting 2 + 1 REMPI line shape summed to give a relative signal S. Power normalization relied upon the results of parallel measurements of the way S varied with laser pulse energy (E), which revealed an $S \propto E^{1.4}$ dependence under our typical operating conditions. This procedure was repeated for some 30 different B_2H_6 flow rates, selected in random order. As Figure 3a shows, the measured B atom signal—which we take to be proportional to the local B atom number density and henceforth represent simply as [B]—is found to increase essentially linearly with the percentage of B_2H_6. Further definitive evidence that the detected B atoms arise as a result of gas-phase chemistry is provided by the data displayed in Figure 3b. This shows two separate measurements of the time decay of the 2 + 1 REMPI signal intensity measured at the peak of the 28886 cm^{-1} feature when a 1 sccm of 4.75% B_2H_6 in H_2 contribution to the total flow is switched to zero. Clearly, [B] falls rapidly, with a 1/e time constant $t \sim 23$ s. Both data sets support the view that B atoms and B_2H_6 molecules are in local thermodynamic equilibrium in the gas phase; the observation that the B atom signal falls to zero within ~100 s of shutting off the 1 sccm 4.75% B_2H_6 in H_2 contribution to the total flow indicates that desorption from the HF makes an immeasurably small contribution to the measured gas-phase B atom signal, even at small d.

Thus, the spatial distribution of B atoms within the reactor at any given T_{fil} should be interpretable in terms of gas-phase B/H chemistry, mediated by the effects of gas flow and the local gas temperature distribution. Figure 4 shows B atom relative number densities measured as a function of distance d from a borodized Ta HF under standard pressure and gas flow conditions, at several different T_{fil} values. Several striking features are evident from these plots. [B] displays a local minimum at $d \sim 0$, at all T_{fil}. This can be understood if the Ta HF (even after several hours conditioning in a B_2H_6/H_2 gas mixture) acts as a sink for gas-phase B containing species. A number of similar measurements involving the standard gas mixture, but activated with either a precarburized Ta filament or a bare Re filament were also carried out. The minimum at $d \sim 0$ was less pronounced in both cases, suggesting that such surfaces are poorer sinks for gas phase B containing species than a bare Ta HF. All such plots show [B] declining relatively little over the d range investigated, implying a lack of efficient, purely gas phase, B atom loss processes. As Figure 4 shows, [B] also exhibits an unusual T_{fil} dependence: it increases with T_{fil} up to ~2100 °C, but declines if T_{fil} is raised further. Figure 5, which shows plots of [B] versus T_{fil} measured at $d = 3$ mm with both a borodized Ta HF and a Re HF, under standard pressure and gas flow conditions, illustrates this trend more clearly. Both data sets suggest that the efficiency of boron accommodation on (or into) the HF surface increases with T_{fil}. SEM and SIMS analysis supports this view, revealing that the thickness of the surface crust on a borodized Ta HF (recall Figure 2) and the B penetration depth both increase with T_{fil}. SEM analysis also provides clear indications of surface melting and recrystallization of this outer skin on the HFs operated at $T_{fil} > 2100$ °C. We note that the observed turn over in [B] correlates with the melting temperatures of boron ($T_{mp} = 2076$ °C[23]) and of TaB ($T_{mp} = 2040$ °C[24]).

Such [B] vs d and [B] vs T_{fil} trends are in marked contrast to that observed for H atoms measured under the same experimental conditions. Very much as reported previously for the case of pure H_2,[18,25] the relative H atom number density, [H], in a B_2H_6/H_2 gas mixture activated with a borodized Ta HF is observed to maximize at $d = 0$, to decline with increasing d, and to rise rapidly with increasing T_{fil}. Illustrative data sets are shown in Figure 6. One noteworthy feature of these data is the T_{fil} value (1500 °C) at which H atoms are first detectable by 2 + 1 REMPI, which is >100 °C lower than that found previously with 20 Torr of pure H_2 activated with a Ta HF—suggesting that borodization (or an increase in surface area that accompanies borodization) enhances the efficiency with which a Ta HF catalyses dissociative adsorption of H_2.

B_2H_6/H_2: Modeling. Interpretation of these data is guided by extension of our previous modeling of the gas-phase chemistry prevailing in activated CH_4/H_2 and $CH_4/NH_3/H_2$ gas mixtures in this same HF reactor.[11−13,26] As before, the reactor is represented in Cartesian coordinates, with the +z-direction parallel to the direction of gas flow and perpendicular to the HF. The center axis of the HF defines the y-axis, and x is orthogonal to both y and z. The modeling considers the volume bounded by $x = \pm 60$ mm, $y = \pm 36$ mm and $z = \pm 60$ mm, with the point (0, 0, 0) defining the center of the HF. $d = 0$ corresponds to the point (0, 0, 1.5 mm). The points (0, 0, −60 mm) and (0, 0, +60 mm) define the gas inlet and outlet positions in the model, where the gas temperature T_{gas} was set at 450 K. The gas temperature values at all other boundaries of the numerical grid were chosen so as to ensure that the far field T_{gas} distribution had approximately spherical symmetry. As in our other recent modeling, [26] $\Delta T = T_{fil} - T_{nf}$ (the temperature drop between the HF surface and the immediate gas phase) was assumed to be a function of T_{fil}, declining from $\Delta T = 500$ K at $T_{fil} = 2700$ K to $\Delta T = 350$ K at $T_{fil} = 2200$ K. Guided by the previous modeling, our 3-D simulations of dilute B_2H_6/H_2 gas mixtures activated by a borodized Ta HF under our standard

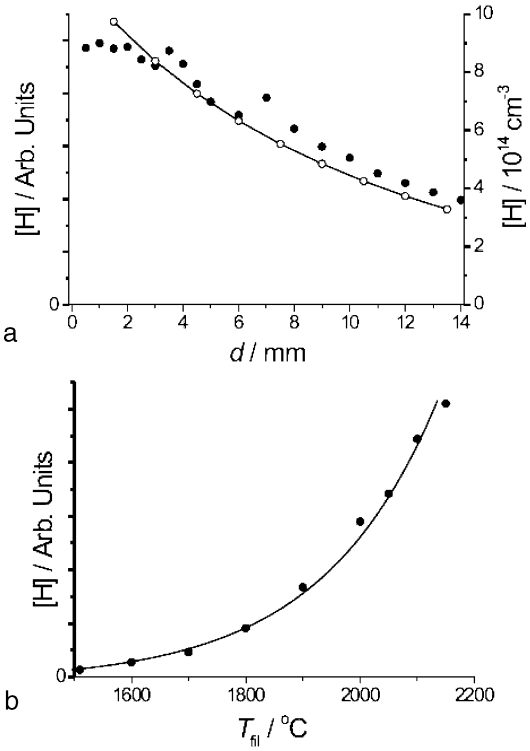

Figure 6. (a) Plot of (relative) [H] measured by 2 + 1 REMPI at 243.1 nm vs d at $T_{fil} = 2100$ °C superimposed on the (absolute) [H] vs d dependence calculated for the specified base conditions. (b) Plot of [H] vs T_{fil} measured at $d = 3$ mm. The line through the data points in part b is merely intended to guide the eye.

operating conditions adopted experimental values for T_{fil}, and the gas pressure and flow rate, and assumed a net H atom production rate at the HF surface $Q = 1.27 \times 10^{19}$ cm^{-2} s^{-1}, a near filament gas temperature $T_{nf} = 1900$ K and a d dependence for T_{gas} analogous to that found in our previous characterizations.[11,12] One additional refinement included in the present modeling was a T_{fil} dependent accommodation coefficient γ for B containing species incident on the HF surface.

The modeling also requires a gas-phase reaction mechanism, and estimates of the relevant temperature and pressure dependent rate constants $k(T, p)$ for the various elementary steps included in the model. The literature contains remarkably little detailed kinetic information pertaining to B/H containing gas mixtures. We start with the minimalist mechanism listed as reactions 1−5 in Table 1. Parameters for reactions 1, 2, and 4 are taken from Harris et al.[16] We have not traced any experimental or theoretical determinations of the rate constant for reaction 3. The parameters given in Table 1 for this reaction were derived by interpolation between those for reactions 2 and 4; the estimated forward rate constant for this H-shifting reaction approaches the limiting gas kinetic collision frequency at high (∼1500 K) temperatures, as should be expected for such a barrierless exothermic process.[16] We have also failed to uncover data for reaction 5, the thermal decomposition of B_2H_6 in H_2, at high (∼1000−2000 K) temperatures. In this preliminary modeling study we have assumed the rate coefficient given in Table 1, and we have assumed an activation energy for the thermal decomposition of B_2H_6 equal to the enthalpy difference between reactants and products. H + B_2H_6 interactions represent another possible initiation step for BH_x radical formation. One such step is the H-shifting reaction H + B_2H_6 ↔ H_2 + B_2H_5 (listed as reaction 6 in Table 1), for which, again, we can find no kinetic data but here assume kinetic parameters as for reaction 4. In equilibrium,

TABLE 1: B/H Reaction Mechanism Used in the Present Work, together with Elements of an Illustrative B/C/H Reaction Scheme[a]

reaction	A, cm$^{3(6)}$ mol^{-1} s^{-1}	B	E, cal mol^{-1}
(1) H + H + H_2 ↔ H_2 + H_2	9.9×10^{16}	−0.6	0.0
(2) H + BH ↔ H_2 + B	1.1×10^{6}	2.3	1671.6
(3) H + BH_2 ↔ H_2 + BH	5.0×10^{5}	2.3	3200.0
(4) H + BH_3 ↔ H_2 + BH_2	1.7×10^{5}	2.8	5731.2
(5) B_2H_6 + H_2 ↔ BH_3 + BH_3 + H_2	2.4×10^{13}	0.0	39000.0
(6) H + B_2H_6 ↔ H_2 + B_2H_5	1.7×10^{5}	2.8	5731.2
(7) BH_3 + C_2H_4 → products	6.0×10^{12}	0.0	0.0
(8) BH_3 + C_2H_2 → products	6.0×10^{12}	0.0	0.0
(9) BH_2 + CH_4 ↔ BH_3 + CH_3	6.0×10^{13}	0.0	0.0

[a] Rate constants are expressed in the traditional form $k = f(A, B, E) = AT^B \exp(-E/RT)$, with units as defined in the column heads and $R = 1.9872$ cal mol^{-1} K^{-1}.

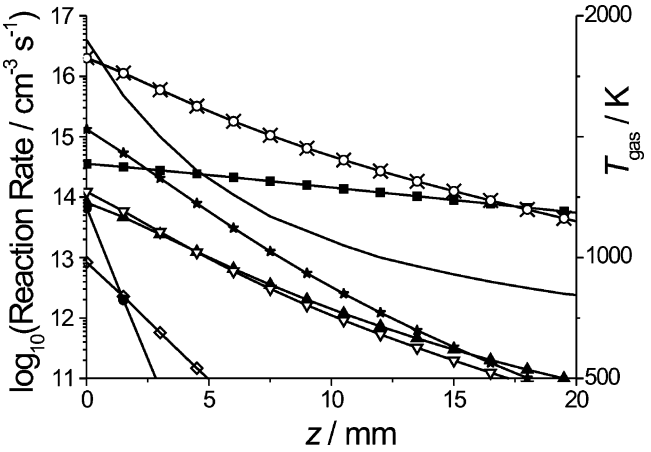

Figure 7. Semilogarithmic plot showing calculated rates, R (in molecules cm^{-3} s^{-1}) for various of the more important elementary reactions in a dilute HF activated 0.05% B_2H_6 in H_2 gas mixture as a function of z (with $x = y = 0$). The calculations assume the following base conditions: 100 sccm total flow rate, $p = 20$ Torr, $T_{nf} = 1900$ K, $Q = 1.27 \times 10^{19}$ cm^{-2} s^{-1} and $\gamma = 0.04$. Key: (■) reaction 1; (●) reaction −1; (▲) reaction 2; (▽) reaction 3; (◇) reaction −3; (×) reaction 4; (○) reaction −4; (★) reaction 5. The assumed z dependence of T_{gas} is illustrated by − and the (linear) scale on the right-hand axis.

at $T_{gas} = 1900$ K and in the presence of a hydrogen atom mole fraction $x(H) = 0.01$, we can then calculate that the B_2H_5 mole fraction $x(B_2H_5)$ might be ∼30% that of $x(B_2H_6)$. Subsequent H + B_2H_y ($y < 6$) reactions e.g. H + B_2H_5 ↔ BH_2 + BH_4 clearly demand future study as possible additional sources of BH_x radicals.

Armed with this simple mechanism, we can predict z (and thus T_{gas}) dependent rates for the various interconversion reactions 1−5 listed in Table 1. Figure 7 shows the results of such a calculation, for the following set of base conditions: 0.05% B_2H_6 in H_2 input gas mixture; 100 sccm total flow rate; $p = 20$ Torr, $T_{nf} = 1900$ K; $Q = 1.27 \times 10^{19}$ cm^{-2} s^{-1} and assuming a modest loss of boron to the HF ($\gamma = 0.04$). The calculations serve to validate the assumed efficiency of the thermal decomposition of B_2H_6 (reaction 5)—which, purely by gas-phase chemistry, is calculated to occur at a rate $>10^{15}$ cm^{-3} s^{-1} near the HF—and rapid interconversion between the various BH_x species driven by the family of H-shifting reactions 2−4:

$$H + BH_x \leftrightarrow H_2 + BH_{x-1}, \quad x = 3-1$$

Guided by the experimental observations, the modeling allows the possibility that gas-phase boron containing species can be

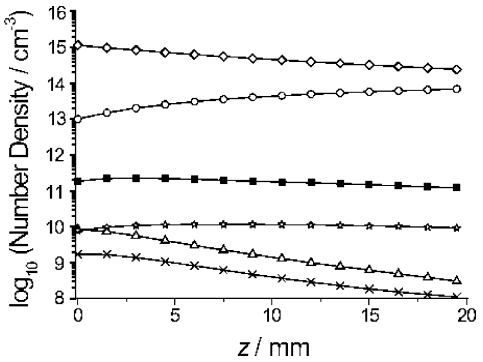

Figure 8. Calculated z dependent number densities of H (◇), B_2H_6 (○), BH_3 (■), BH_2 (△), BH (×), and B (☆) in a 0.05% B_2H_6 in H_2 input gas mixture employing the same base conditions as in Figure 7.

lost, irreversibly, by incorporation into the HF. However, it does not allow for possible BH_x ($x = 0-3$) production by, for example, dissociative absorption of B_2H_6 on the HF surface—such as has been invoked in some earlier analyses of C_2H_4 decomposition.[27] The rate of loss of boron containing species at the HF was modeled by eq 2

$$G = {}^1/_4 \gamma N_i \upsilon S \qquad (2)$$

where S is the effective surface area of the filament in the grid cell, N_i is the relevant species number density close to the filament, υ is the thermal velocity of this species, and γ is the probability that collision with the HF surface will result in irreversible loss of that species from the gas phase. γ for the various boron containing species was assumed to be equal to that for atomic B. Setting $\gamma > 0$ has the effect of reducing the number densities of the various boron containing species (particularly in the immediate vicinity of the HF) and thus reducing the rates R of all reactions involving such species.

This can be appreciated more clearly from the calculated T_{gas} (and thus d) dependent species number densities. Figure 8 shows calculated d dependent number densities for H, BH_x ($x = 0-3$) and B_2H_6 for the same base conditions as used in Figure 7. We should stress at this point that the quoted number densities are correct for the kinetic parameters listed in Table 1, but could change significantly if new, accurate data relating to B_2H_6 conversion to BH_x species (by thermal decomposition and/or reaction with H atoms) became available. The present calculations show B_2H_6 dissociation to BH_3 near the HF such that $N(BH_3) > 1\%$ $N(B_2H_6)$ at $d \sim 0$, and efficient conversion of the BH_3 species so formed to BH_2, BH and, particularly, B atoms via the sequence of H-shifting reactions 2−4. The calculations also show that N(B) varies less steeply with d than do either $N(BH_2)$ or N(BH). The calculated d dependence of N(B) is comparatively "flat" , in general agreement with the [B] vs d trend measured experimentally, though the calculations also show that $\gamma > 0$ is required in order to obtain a local minimum in N(B) at $d \sim 0$. This effect is illustrated further in Figure 9, in which the measured [B] vs d trend with a borodized Ta HF at $T_{fil} = 2100$ °C (from Figure 4) has been superimposed on a range of N(B) vs d distributions calculated for the usual base conditions but with a range of different γ values. The observed [B] vs T_{fil} trends can be reproduced reasonably well using the previously determined $Q(T_{fil})$ dependence if γ is allowed to scale with T_{fil} as shown in the inset to Figure 5. Clearly, γ is required to increase quite dramatically at filament temperatures above ~2100 °C, i.e. at temperatures when the filament surface could support a thin layer of molten boron.

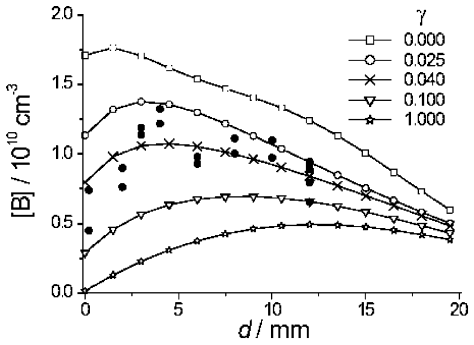

Figure 9. [B] vs d trend measured in a borodized Ta HF activated 0.0475% B_2H_6 in H_2 gas mixture ($T_{fil} = 2100$ °C, from Figure 4) superimposed on various N(B) vs d distributions calculated assuming the base conditions listed in the caption to Figure 7 but with a range of γ values.

Effect of CH_4 Additions. Inclusion of CH_4 within the process gas mixture introduces more variables. Clearly, H/B/C containing mixtures can support a wider range of gas-phase chemistry than the simpler H/B mixtures. Additionally, however, B and C containing species can both react—competitively and, conceivably, cooperatively—with the surface of a HF. To minimize this potential variability, we chose to adopt a standard operating procedure in which a new Ta HF was first carburized at $T_{fil} = 2250$ °C in a 1% CH_4/H_2 gas mixture for 6 h prior to exposure to any B_2H_6. Carburized HFs were used to activate both B_2H_6/H_2 gas mixtures (results of some such experiments have been described above) and $B_2H_6/CH_4/H_2$ mixtures. In both cases, B atoms were detectable as soon as B_2H_6 was introduced, and the measured [B] vs d dependences were reminiscent of those found with a Re HF − implying that B accommodation on a precarburized surface is relatively inefficient (small γ). In marked contrast to the situation found with the bare metal filaments, however, [B] was found to rise more than linearly with increasing T_{fil}, with no sign of a turn-over at $T_{fil} \sim 2100$ °C (Figure 10a), though [B] does appear to plateau at $T_{fil} \sim 2300$ °C. This we rationalize in terms of formation of a thin (solid) borocarbide surface layer, rather than the molten B coating (or TaB, or hydrogenated variants thereof) deduced in the case of the borodized metal HFs at high T_{fil}. Given these observations, one might argue that a precarburized HF should be the filament of choice for this type study. However, the precarburization stage is time-consuming, and the resulting coating is delicate. Such filaments are not recyclable, since the thermal stresses associated with cooling (to room temperature) and reheating are sufficient to crack the carbonaceous coating, thereby exposing bare metal that has to be recarburized prior to use. After completion of the precarburization stage, the temperatures of the HFs used in the experiments reported here were only reduced when conducting [B] vs T_{fil} profiles (during which T_{fil} was still maintained at >1600 °C).

Figure 10b shows the time dependence of the B atom signal measured at $d = 3$ mm with a precarburized Ta HF maintained at $T_{fil} = 2250$ °C, as a function of CH_4 addition. The B atom number density measured in a 0.0475% B_2H_6 in H_2 mixture is seen to fall by >30% upon addition of 1% CH_4, but quickly recovers its previous value when the CH_4 flow is interrupted. Given the reproducibility of this trend, the lack of obvious hysteresis in the data, or of any change in T_{fil} upon CH_4 addition, we conclude that the observed variation in [B] is due to gas-phase chemistry. We now consider possible causes for the observed variation upon CH_4 addition.

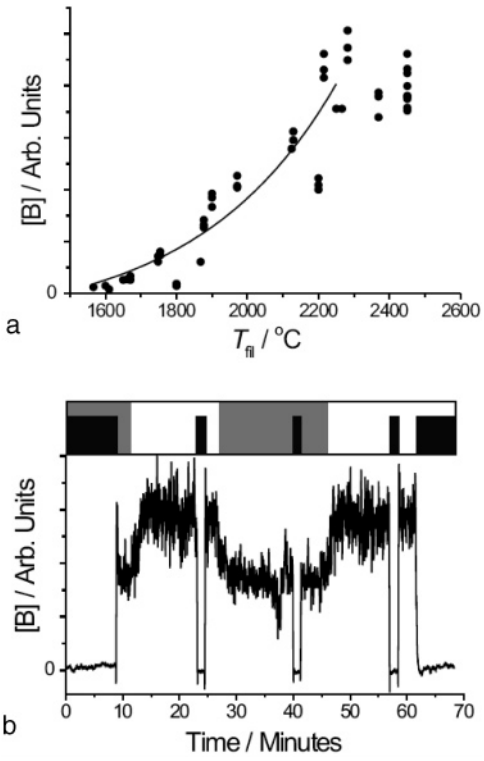

Figure 10. (a) Plot of [B] vs T_{fil} measured at $d = 3$ mm when using a 0.0475% B_2H_6/1% CH_4/H_2 gas mixture and a precarburized Ta HF. The line through the data at $T_{fil} \leq 2250$ °C is simply to guide the eye. (b) Plot of [B] vs time measured at $d = 3$ mm with a precarburized Ta HF maintained at $T_{fil} = 2250$ °C, using a 0.0475% B_2H_6/*x*% CH_4/H_2 mixture in which *x* is alternated from 0 to 1—represented by, respectively, the periods of white and gray shading on the time-bar above. Black regions on this time bar indicate periods when the probe laser was blocked.

The literature regarding B/C coupling reactions in the gas phase is comparatively sparse. Andrews and co-workers, using matrix isolation methods, identified CH_2BH_2 and CH_2BH as products of the reaction of B atoms with CH_4.[28] Formation of these products was rationalized in terms of an initial exothermic insertion reaction, yielding CH_3BH, and subsequent rearrangement to the thermodynamically favored isomer CH_2BH_2 and/or H atom elimination prior to the excess internal energy being dissipated into the matrix.[29] The B atoms in that experiment were generated by pulsed Nd:YAG laser ablation of a solid boron target; their average kinetic energy was estimated at ~110 kcal mol^{-1}.[30] The high collision energies are very relevant, since subsequent ab initio calculations[31,32] have revealed a substantial energy barrier in the entrance channel of the B + CH_4 reaction, the magnitude of which (~20.8 kcal mol^{-1} (ref 31)) would preclude reaction at room temperature. This reaction is thus unlikely to account for the observed drop in [B] upon CH_4 addition to the HF activated B_2H_6/H_2 gas mixture. HF activation of CH_4/H_2 mixtures leads to C_2H_2 formation.[13] The B + C_2H_2 reaction has been investigated by matrix isolation methods also[33] and, more recently, in crossed-beam reactive scattering experiments.[34,35] The latter reveal HBC_2 as the sole molecular product; companion ab initio calculations suggest an indirect formation mechanism involving (barrierless) B atom addition to the C≡C triple bond, subsequent cyclic rearrangement involving an H atom migration, isomerization to a ring opened structure, and eventual H atom loss to yield the observed HBCC product. This reaction is calculated to be mildly exothermic, $\Delta_r H = -1.6$ kcal mol^{-1}. Would the HBCC species be sufficiently stable to act as a sink for gas phase B atoms under conditions typically found during diamond CVD?

Given that the efficiency of interconversion between the various BH_x species via the H-shifting reactions 2−4 is rapid, loss of any BH_x species could, in principle, account for the observed decline in [B] upon addition of CH_4. Figure 8 showed BH_3 to be the most abundant BH_x species, at all *d*. BH_3 is not expected to react with CH_4 itself. Diode laser absorption studies of the $BH_3 + C_2H_4$ reaction returned BH_3 removal rate constants $> 10^{-11}$ cm^3 s^{-1}, at room temperature and at N_2 buffer gas pressures as low as 6 Torr,[36] while previous flow-tube studies suggested that the adduct, ethylborane, was the major reaction product.[37] Theory generally supports this view, though the reliability of the early picture of the reaction proceeding via a two-step mechanism involving initial π-complex formation and subsequent rearrangement via a four center transition state has been called into question by higher level calculations which suggest a steady decline in energy with decreasing $BH_3-C_2H_4$ separation.[38] BH_3 addition to C_2H_2 (which will be the most abundant hydrocarbon in the hottest regions of any HF activated dilute CH_4/H_2 gas mixture) appears to have received relatively little experimental attention, but is a recognized route to forming vinylborane. Theory suggests that the $BH_3 + C_2H_2$ and $BH_3 + C_2H_4$ reactions should show many similarities. Again, the π-complex is predicted to be stable (by ~3.3 kcal mol^{-1} relative to the separated reactants), and the barrier associated with the subsequent transition state for H migration is predicted to be a mere 2 kcal mol^{-1} measured relative to the π-complex; the overall exothermicity of vinylborane product formation from $BH_3 + C_2H_2$ is calculated to be ~43.6 kcal mol^{-1}.[39] Neither C_2H_2 nor C_2H_4 are expected to react significantly with B_2H_6 in the gas phase at room temperature.

Clearly, our current understanding of possible gas-phase B/C coupling reactions under conditions representative of those used in boron-doped diamond CVD is far from adequate. Nonetheless, we have performed some preliminary model calculations appropriate to the near HF region in the present reactor. Specifically, for 0.0475% B_2H_6/H_2 and 1% CH_4/H_2 gas mixtures, we find $[BH_3] \sim 10^{11}$ cm^{-3} and $[C_2H_2] \sim 2 \times 10^{13}$ cm^{-3} and $[C_2H_4] \sim 10^{12}$ cm^{-3}, at $d \sim 3$ mm. Assuming that these number densities would be replicated in a HF activated 0.0475% $B_2H_6/$1% CH_4/H_2 gas mixture, we would require that reactions 7 and 8 in Table 1 removed BH_3 with essentially unit collision efficiency ($k \sim 10^{-10}$ cm^3 s^{-1}, at $T_{gas} \sim 1500-1900$ K and $p(H_2) = 20$ Torr) in order to give a reaction rate ($\sim 2 \times 10^{14}$ cm^{-3} s^{-1}) sufficient to account for the observed 30% loss of B atoms upon CH_4 addition to a HF activated 0.0475% B_2H_6/H_2 gas mixture. The resulting vinylborane and ethylborane products will almost certainly react further, given the high ($> 10^{14}$ cm^{-3}) H atom number densities, and much further work will be required to establish the complete set of gas phase (and reactor surface) sinks for the boron introduced into CH_4/H_2 gas mixtures used to grow B-doped diamond. Other $BH_x + CH_y$ type reactions (e.g., $BH_2 + CH_4 \leftrightarrow BH_3 + CH_3$) could, in principle, lead to reductions in the BH_x ($x = 2-0$) reactant concentrations. Again, we estimate that the rate coefficients of any such reactions would need to be $\sim 10^{-10}$ cm^3 s^{-1} in order to be competitive with reaction −4, $k_{-4} \sim 10^{-11}$ cm^3 s^{-1}.

On the basis of these calculations, none of the above B/C coupling reactions provides a convincing explanation for the level of [B] depletion observed upon addition of 1% CH_4 to the 0.0475% B_2H_6/H_2 gas mixture. However, preliminary 2-D(*r*, *z*) model calculations for $T_{nf} = 1900$ K outputs for a HF activated 0.05% B_2H_6/H_2 gas mixture assuming reactions 1−6

from Table 1, and a 0.05% B_2H_6/1% CH_4/H_2 mixture in which we allow the full B/H chemistry (i.e. reactions 1−6 again), and the full C/H chemistry associated with the 12 CH_x and C_2H_x species assumed in previous modeling of HF activated CH_4/H_2 gas mixtures,[13] and the B/C coupling reactions 7−9, suggests an alternative explanation. These predict a ∼45% drop in [B], as compared with the simple B/H chemistry, in very reasonable accord with the >30% decrease observed experimentally. The predicted rates of reactions 7, 8, and 9 are, respectively, $\sim 10^{14}$, 10^{14}, and 10^{15} cm^{-3} s^{-1} at $d < 10$ mm. Reaction 9 and the reverse reaction (reaction −9) are almost in balance; the difference in their respective rates, $R(9) - R(-9)$, is $\sim 10^{14}$ cm^{-3} s^{-1}. CH_4 introduces additional H atom loss processes (i.e. the sequence of $CH_x + H \leftrightarrow CH_{x-1} + H_2$ H-shifting reactions). [H] at small d is calculated to drop by ∼20%. This has relatively little effect on the calculated $[BH_3]$—which is largely determined by the thermal dissociation of B_2H_6, but has a progressively greater effect on each of the subsequent $BH_x + H \leftrightarrow BH_{x-1} + H_2$ H-shifting reactions 2−4, leading to the predicted (and observed) reduction in [B].

Conclusions

This paper describes new experimental and companion modeling studies of the gas-phase chemistry occurring in dilute, HF activated B_2H_6/H_2 and $B_2H_6/CH_4/H_2$ gas mixtures. Here, 2 + 1 REMPI methods have been used to measure spatially resolved relative number densities of B (and H) atoms, as a function of process conditions. The B atom number density in a Ta HF activated B_2H_6/H_2 mixture shows a local minimum in the immediate vicinity of the HF. This, and the observed turn over in [B] with increasing T_{fil}, can both be rationalized by assuming a (T_{fil} dependent) accommodation efficiency for B (and other BH_x) species incident on the HF surface. The 3-D modeling of the H/B chemistry prevailing in an HF activated B_2H_6/H_2 gas mixture employing a simplified representation of the gas-phase chemistry succeeds in reproducing the trends observed experimentally, and it highlights the key role of the various H-shifting reactions $BH_x + H \rightleftharpoons BH_{x-1} + H_2$ ($x = 1-3$) in encouraging rapid interconversion between the various BH_x ($x = 0-3$) species. Addition of CH_4 at a partial pressure appropriate for growth of B-doped diamond by CVD methods, causes a ∼30% reduction in [B] near the HF. The preliminary modeling undertaken thus far suggests that this observation is largely attributable to the concomitant depletion of the H atom number density near the HF upon CH_4 addition, but it also highlights the paucity of the available kinetic data for possible B/C coupling reactions in thermally activated $B_2H_6/CH_4/H_2$ gas mixtures.

Acknowledgment. We are grateful to EPSRC for the award of a portfolio grant (LASER) and for postdoctoral support via the Carbon Based Electronics initiative (J.A.S.), Element Six Ltd for the award of an Industrial CASE studentship (A.C.), the Institute of Advanced Studies at University of Bristol for the award of a Benjamin Meaker Visiting Professorship (Y.A.M.), the Royal Society for a Joint Project Grant that enables the Bristol−Moscow collaboration, and Dr. P. Heard (Interface Analysis Centre, University of Bristol), and School of Chemistry colleagues Drs. C. M. Western and K. N. Rosser for their many and varied contributions to the work described herein.

References and Notes

(1) Deneuville, A. *Semicond. Semimet.* **2003**, *76*, 183 and references therein.
(2) Isberg, J.; Hammersberg, J.; Johansson, E.; Wikström, T.; Twitchen, D. J.; Whitehead, A. J.; Coe, S. E.; Scarsbrook, G. A. *Science* **2002**, *297*, 1670.
(3) Angus, J.; Pleskov, Y. V.; Eaton, S. C. *Semicond. Semimet.* **2004**, *77*, 97 and references therein.
(4) Koizumi, S.; Watanabe, K.; Hasegawa, F.; Kanda, H. *Science* **2001**, *292*, 1899.
(5) Teukam, Z.; Chevallier, J.; Saguy, C.; Kalish, R.; Ballutaud, D.; Barbé, M.; Jomard, F.; Tromson-Carli, A. Cytermann, C.; Butler, J. E.; Bernard, M.; Baron, C.; Deneuville, A. *Nat. Mater.* **2003**, *2*, 482.
(6) Goss, J. P.; Briddon, P. R.; Sque, S. J.; Jones, R. *Phys. Rev. B* **2004**, *69*, 165215.
(7) Samlenski, R.; Haug, C.; Wild, C.; Locher, R.; Koidl, P. *Diam. Relat. Mater.* **1996**, *5*, 947.
(8) Wurzinger, P.; Pongratz, P.; Hartmann, P.; Haubner, R.; Lux, B. *Diam. Relat. Mater.* **1997**, *6*, 763.
(9) Cheesman, A.; Harvey, J. N.; Ashfold, M. N. R. *Phys. Chem. Chem. Phys.* **2005**, *7*, 1121.
(10) Mankelevich, Y. A.; Rakhimov, A. T.; Suetin, N. V. *Diam. Relat. Mater.* **1998**, *7*, 1133.
(11) Smith, J. A.; Cameron, E.; Ashfold, M. N. R.; Mankelevich, Y. A.; Suetin, N. V. *Diam. Relat. Mater.* **2001**, *10*, 358.
(12) Mankelevich, Y. A.; Suetin, N. V.; Ashfold, M. N. R.; Smith, J. A.; Cameron, E. *Diam. Relat. Mater.* **2001**, *10*, 364.
(13) Ashfold, M. N. R.; May, P. W.; Petherbridge, J. R.; Rosser, K. N.; Smith, J. A.; Mankelevich, Y. A.; Suetin, N. V. *Phys. Chem. Chem. Phys.* **2001**, *3*, 3471.
(14) Mankelevich, Yu. A.; Suetin, N. V.; Smith, J. A.; Ashfold, M. N. R. *Diam. Relat. Mater.* **2002**, *11*, 567.
(15) Schlegel, H. B.; Baboul, A. G.; Harris, S. J. *J. Phys. Chem.* **1996**, *100*, 9774.
(16) Harris, S. J.; Kiefer, J.; Zhang, Q.; Schoene, A.; Lee, K. W. *J. Electrochem. Soc.* **1998**, *145*, 3203.
(17) Yu, C.-L.; Bauer, S. H. *J. Phys. Chem. Ref. Data* **1998**, *27*, 807 and references therein.
(18) Redman, S. A.; Chung, C.; Rosser, K. N.; Ashfold, M. N. R. *Phys. Chem. Chem. Phys.* **1999**, *1*, 1415.
(19) NIST Atomic Spectra Database, http://physics.nist.gov/cgi-bin/AtData/main_asd.
(20) Irikura, K. K.; Johnson, R. D.; Hudgens, J. W. *J. Opt. Soc. Am. B* **1993**, *10*, 763.
(21) DRIVE, written and maintained by Western, C. M., University of Bristol.
(22) Lavrov, B. P.; Osiac, M.; Pipa, A. V.; Röpcke, J. *Plasma Sources Sci. Technol.* **2003**, *12*, 576.
(23) http://www.webelements.com/webelements/elements/text/B/heat.html.
(24) Samsonov, G. V.; Markivskii, L. Y. *Uspekhi Khim.* **1956**, *25*, 190.
(25) Smith, J. A.; Cook, M. A.; Langford, S. R.; Redman, S. A.; Ashfold, M. N. R. *Thin Solid Films* **2000**, *368*, 169.
(26) Smith, J. A.; Wills, J. B.; Moores, H. S.; Orr-Ewing, A. J.; Ashfold, M. N. R.; Mankelevich, Y. A.; Suetin, N. V. *J. Appl. Phys.* **2002**, *92*, 672.
(27) Winters, H. F.; Seki, H.; Rye, R. R.; Coltrin, M. E. *J. Appl. Phys.* **1994**, *76*, 1228.
(28) Hassanzadeh, P.; Hannachi, Y.; Andrews, L. *J. Phys. Chem.* **1993**, *97*, 6418.
(29) Hannachi, Y.; Hassanzadeh, P.; Andrews, L. *J. Phys. Chem.* **1994**, *98*, 6950.
(30) Tague, Jr., T. J.; Andrews, L. *J. Am. Chem. Soc.* **1994**, *116*, 4970.
(31) Fang, W.-H.; Peyerimhoff, S. D. *Mol. Phys.* **1998**, *93*, 329.
(32) Wang, Z.-X.; Huang, M.-B. *J. Am. Chem. Soc.* **1998**, *120*, 6758.
(33) Andrews, L.; Hassanzadeh, P.; Martin, J. M. L.; Taylor, P. R. *J. Phys. Chem.* **1993**, *97*, 5839.
(34) Balucani, N.; Asvany, O.; Lee, Y. T.; Kaiser, R. I.; Galland, N.; Rayez, M. T.; Hannachi, Y. *J. Comput. Chem.* **2001**, *22*, 1359.
(35) Kaiser, R. I.; Balucani, N.; Galland, N.; Caralp, F.; Rayez, M. T.; Hannachi, Y. *Phys. Chem. Chem. Phys.* **2004**, *6*, 2205.
(36) Pasternack, L.; Balla, R. J.; Nelson, H. H. *J. Phys. Chem.* **1988**, *92*, 1200.
(37) Fehlner, T. P. *Int. J. Chem. Kinet.* **1975**, *7*, 633.
(38) Wang, X.; Li, Y.; Wu, Y.-D.; Paddon-Row: M. N.; Rondan, N. G.; Houk, K. N. *J. Org. Chem.* **1990**, *55*, 2601.
(39) McKee, M. L. *J. Am. Chem. Soc.* **1995**, *117*, 8001.